Journal of Solid State Chemistry **161,** 31–37 (2001)
doi:10.1006/jssc.2001.9243, available online at http://www.idealibrary.com on IDEAL®

Nonstoichiometric, Rutile-Type, Solid Solutions in the $Fe^{II}F_2$–$Fe^{III}OF$ System

Frank J. Brink,[1] Ray L. Withers,[2] and Lasse Norén

Research School of Chemistry, Australian National University, Canberra, ACT 0200, Australia

Received January 25, 2001; in revised form April 18, 2001; accepted May 11, 2001; published online August 24, 2001

Solid solutions of the form $Fe^{II}_{(1-x)}Fe^{III}_xO_xF_{2-x}$ have been synthesized by the reaction of FeF_2 with FeOF in a sealed platinum tube at 850°C. Careful electron probe microanalysis and X-ray powder diffraction have determined the existence of two distinct solid solution regions extending from $0 \leq x \leq 0.08$ at the $Fe^{II}F_2$ end and from $0.71 \leq x \leq 1$ at the $Fe^{III}OF$ end with a miscibility gap from $0.08 \leq x \leq 0.71$. Electron diffraction experiments have revealed the presence of characteristic diffuse intensity distributions for samples within either solid solution region. Plausible explanations for the observed diffraction phenomena, based upon crystal chemical and bond length–bond valence arguments, are provided. © 2001 Academic Press

INTRODUCTION

Investigation into oxygen/fluorine substitution and associated nonstoichiometry in oxyfluoride systems has long been of interest, both from the fundamental point of view but also because the physicochemical properties of such phases are often strongly dependent upon the extent of such substitution (1–6). The similarity in size of oxide, O^{2-}, and fluoride, F^-, anions suggests the possibility of ready substitution of one anion for the other and, in principle, should favor the formation of wide-range, nonstoichiometric solid solutions with the same average structure type. On the other hand, the charge and electronegativity differences between O^{2-} and F^- anions might be expected to provide a driving force for oxygen/fluorine ordering at simple composition ratios and to act against the existence of wide-range, nonstoichiometric solid solutions.

Most oxyfluoride systems to date, whether line phases or solid solutions, have been reported to exhibit a statistical distribution of O^{2-} and F^- at the anion sites, mainly as a result of the difficulty in distinguishing between oxygen and fluorine via direct diffraction techniques (3). By contrast, spectroscopic and local bonding considerations (3) have often suggested that oxygen/fluorine ordering must be occurring, at least on a local scale. A recent electron diffraction investigation (7) of stoichiometric rutile-type $Fe^{III}OF$, for example, one of the simplest of the known metal oxyfluoride structure types (see Fig. 1), found clear evidence for long-range ordering of O^{2-} and F^- anions within {110} planes but without any correlation from one such {110} plane to the next. This observation enabled apparently contradictory results about oxygen/fluorine ordering obtained from single-crystal X-ray diffraction and Mössbauer spectroscopy to be reconciled.

Given that both $Fe^{III}OF$ and $Fe^{II}F_2$ have rutile-type average structures ($P4_2/mnm$, $a = 4.64317(7)$ and $c = 3.0436(5)$ Å for FeOF (7) and $a = 4.6974$ and $c = 3.3082$ Å for FeF_2 (8)) with very similar a cell dimensions, albeit with their respective c dimensions differing by $\sim 10\%$, it seemed logical to extend this previous work to the investigation of solid solutions of the form $Fe^{II}_{(1-x)}Fe^{III}_xO_xF_{2-x}$ found in the FeF_2–FeOF system. The existence of solid solutions of this type was first mentioned by Hagenmuller *et al.* (9) who reported a solid solution range $0 \leq x \leq 0.18$ at the $Fe^{II}F_2$ end and $0.92 \leq x \leq 1$ at the $Fe^{III}OF$ end with the existence of a miscibility gap for $0.18 < x < 0.92$.

In this earlier work, however, there was no mention of how the composition of the various synthesized specimens was determined. Since the presence of adsorbed surface water is almost unavoidable in transition metal fluorides (10) and leads to the evolution of HF gas on heating, the absolute composition of resultant rutile-type metal oxyfluorides cannot be reliably inferred from nominal starting compositions, but should instead be determined through subsequent analysis of the reaction product. In this study we therefore concentrate on determining the solid solution range at either end via electron microprobe analysis (EPMA) using stoichiometric FeOF as a compositional standard and upon electron diffraction investigation of the synthesized specimens to search for evidence of the oxygen/fluorine and/or Fe^{2+}/Fe^{3+} substitution mechanism.

[1]Also at Electron Microscope Unit, Research School of Biological Sciences, Australian National University, Canberra, ACT 0200, Australia.
[2]To whom correspondence should be addressed.

0022-4596/01 $35.00

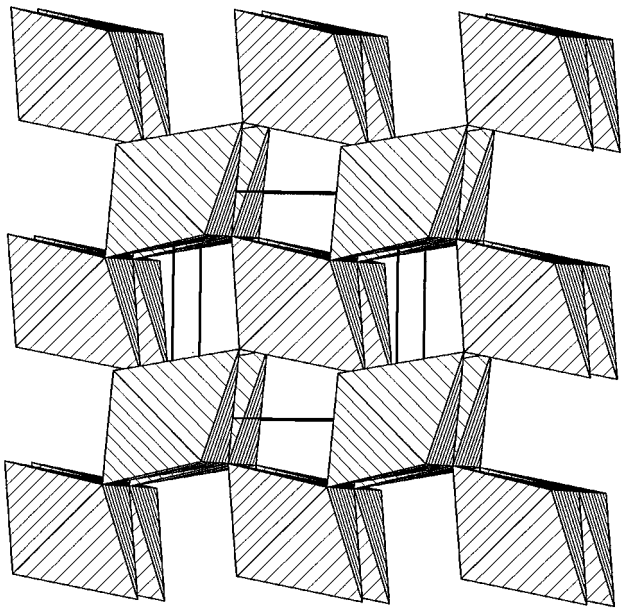

FIG. 1. 3-D projection of the FeOF rutile-type average structure. The FeA_6 (A = anion) octahedra are shown hatched. The unit cell is outlined in the center.

EXPERIMENTAL

Synthesis

A range of $Fe^{II}_{(1-x)}Fe^{III}_xO_xF_{2-x}$ solid solution compositions were synthesized by the reaction of FeF_2 (Cerac, 99.5% nominally anhydrous) with previously synthesized FeOF (7) in a sealed platinum tube at 850°C for 3 to 5 hrs. All reactants were manipulated in an argon-filled drybox to minimize contamination with air or water vapor.

Attempts to react the components at higher temperatures or for longer times led to failure of the platinum tubes. This was attributed to the presence of adsorbed surface water on the FeF_2 which inevitably hydrolyzed during the synthesis, forming HF gas (10). The resultant increase in pressure in the platinum tubes then led to tube failure if the temperature was too high or the reaction time too long.

Qualitative analysis of the FeF_2 by Fourier transform infrared spectrometry (FTIR) confirmed the presence of adsorbed water in the commercial reactant. The unavailability (as far as the reaction forming $Fe^{II}_{(1-x)}Fe^{III}_xO_xF_{2-x}$ is concerned) of an unknown quantity of fluorine in the form of HF gas makes it impossible to predetermine the exact composition of the resultant $Fe^{II}_{(1-x)}Fe^{III}_xO_xF_{2-x}$ specimen from the nominal starting compositions of the reactants.

X-ray Powder Diffraction (XRD), Transmission Electron Microscopy (TEM), and Electron Probe Microanalysis (EPMA)

XRD data collected from a Guinier-Hägg camera ($\lambda = 1.5406$ Å), using an internal Si (NBS #640) standard, were used for phase analysis and to refine unit cell parameters. Samples suitable for transmission electron microscope (TEM) work were prepared by the dispersion of finely ground material onto a holey carbon film. Electron diffraction patterns (EDP's) were obtained using a Philips 430 TEM.

Electron probe microanalysis (EPMA) was used to determine composition. Samples were prepared by mounting them in resin followed by polishing to <1 μm. The analyses were carried out at 15 kV and 1 nA using a JEOL 6400 scanning electron microscope (SEM) equipped with an Oxford Instruments light element EDS detector and Link ISIS SEMquant software. In order to minimize the atomic number, absorption, and fluorescence (ZAF) corrections (11), stoichiometric FeOF was used as a calibration standard throughout.

RESULTS AND DISCUSSION

Electron Probe Microanalysis and XRD

X-ray investigation combined with EPMA confirmed the existence of two distinct $Fe^{II}_{(1-x)}Fe^{III}_xO_xF_{2-x}$ solid solution regions, one at either end of the overall composition range and separated by a clear two-phase region, as first reported by Hagenmuller *et al.* (9). Careful EPMA analysis, using end member FeOF as a standard, was employed to determine the composition range of these two solid solutions. The particle sizes of the reaction products were generally in excess of 50 μm, enabling accurate analysis on individual grains in the SEM. For syntheses within the two-phase region, both end member products were generally well separated and easily identified by their composition.

The compositional extent of the first type of solid solution region (labeled SS1 hereafter) was found to range from $0 \leq x \leq \sim 0.08$, while that of the second type of solid solution (labeled SS2 hereafter) was found to range from $0.71 \leq x \leq 1$. A clear miscibility gap was present from $\sim 0.08 < x < 0.71$. These compositional ranges differ significantly from those initially reported by Hagenmuller *et al.* (9); in particular the compositional range of SS1 was found to be considerably narrower while that of SS2 was found to be significantly broader (see Fig. 2).

The earlier work of Hagenmuller *et al.* (9) suggested that the *a* rutile-type unit cell dimension of these solid solutions changes only very slowly with composition while the *c* dimension, by contrast, changes quite drastically with composition. Given that the *a* cell dimensions of $Fe^{III}OF$ and $Fe^{II}F_2$ differ by only $\sim 1\%$ whereas their *c* cell dimensions differ by $\sim 9\%$, this is not surprising and makes the *c* unit cell dimension a very useful and sensitive measure of composition.

Figure 2 shows the dependency of this rutile-type *c* unit cell dimension upon composition, as determined from our combined EPMA and XRD results. Note the rather broad

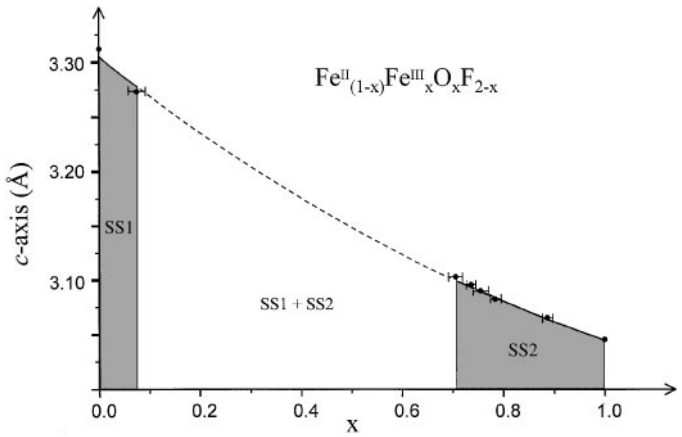

FIG. 2. Plot showing the variation in the c unit cell dimension with composition.

compositional range of the SS2 solid solution in comparison with the rather narrow compositional range of the SS1 solid solution. The rather narrow compositional extent of the SS1 region in conjunction with the volatility of the commercial FeF_2 ruled out synthesis of specimens at a range of compositions within this region. In addition, the low concentration of oxygen ($\sim$1.4% by weight) and an increased deviation away from our analytical standard (FeOF) made it more difficult to obtain accurate analyses ($\pm$20% relative accuracy) at this end of the two-phase region. Analyses within the SS2 region were rather more reliable ($\pm$3% relative accuracy). Note the rather smooth variation in c dimension with composition, which to a first approximation obeys Vegard's law (12). It is also interesting to note that all the data (SS1 inclusive) can be fitted to a single curve despite the existence of a miscibility gap.

The experimental result that the compositional extent of the SS1 region is rather more limited than that of the SS2 region can be considered to be quite sensible from the point of view of local crystal chemistry. Apparent valence (AV) calculations (13) derived from the average structures of both FeF_2 (8, 14) and FeOF (15) (see Table 1), for example, show that an oxygen ion would be severely underbonded (AV = 1.20 valence units, i.e., 0.8 valence unit less than the ideal AV of 2.0) in the average structure anion position of FeF_2 while a fluorine ion substituting for an oxygen ion would be only slightly overbonded (AV = 1.22 instead of the ideal AV of 1.0) in the average structure anion position of FeOF. Similarly, an Fe^{3+} ion substituting for an Fe^{2+} ion in FeF_2 would be extremely underbonded (AV = 2.01 instead of 3.0) whereas an Fe^{2+} ion substituting for an Fe^{3+} ion in FeOF, although significantly overbonded (AV = 2.61), would be rather less removed from its ideal AV of 2.0.

From a crystal chemical point of view it is therefore easier to substitute an $Fe^{II}F_2$ unit for an $Fe^{III}OF$ unit in FeOF than it is to substitute an $Fe^{III}OF$ unit for an $Fe^{II}F_2$ unit in FeF_2. This, we believe, is reflected in the experimentally observed relative compositional widths of the two solid solution fields (see Fig. 2).

Electron Diffraction

Given the earlier electron diffraction evidence for O^{2-}/F^- ordering in the FeOF end member of SS2 (7), electron diffraction has again been employed to look for weak features of reciprocal space that might contain diffraction evidence for O^{2-}/F^- and/or Fe^{2+}/Fe^{3+} ordering within the rutile-type average structure of these two solid solutions. We begin with the SS2 solid solution field.

TABLE 1
Bond Valence Sums (13) for FeF_2 and FeOF ($v_{ij} = \exp[R_{ij} - d_{ij})/b]$, with $b = 0.37$ Å)

FeF_2		Fe^{2+} (6F)	Fe^{3+} (6F)	F ($3Fe^{2+}$)	O ($3Fe^{2+}$)
distance (d_{ij}) Fe–F, O (Å)	R_{ij}	1.650	1.670	1.650	1.734
2×2.002	v M–F, O	2×0.386	2×0.408	2×0.386	1×0.485
4×2.116	v M–F, O	4×0.284	4×0.299	2×0.284	2×0.356
	$V_i = \Sigma v_{ij}$	1.91	2.01	0.95	1.20
	V_i (theor.)	2.00	3.00	1.00	2.00
FeOF		Fe^{2+} (3F, 3O)	Fe^{3+} (3F, 3O)	F ($3Fe^{3+}$)	O ($3Fe^{3+}$)
distance Fe–F, O (Å)	R_{ij}	1.650 (F)	1.670 (F)	1.670 (F)	1.759 (O)
		1.734 (O)	1.759 (O)		
2×1.986	v M–F, O	1×0.403	1×0.425	1×0.426	1×0.541
		1×0.506	1×0.541		
4×2.010	v M–F, O	2×0.378	2×0.399	2×0.399	2×0.508
		2×0.474	2×0.508		
	$V_i = \Sigma v_{ij}$	2.61	2.78	1.22	1.56
	V_i (theor.)	2.00	3.00	1.00	2.00

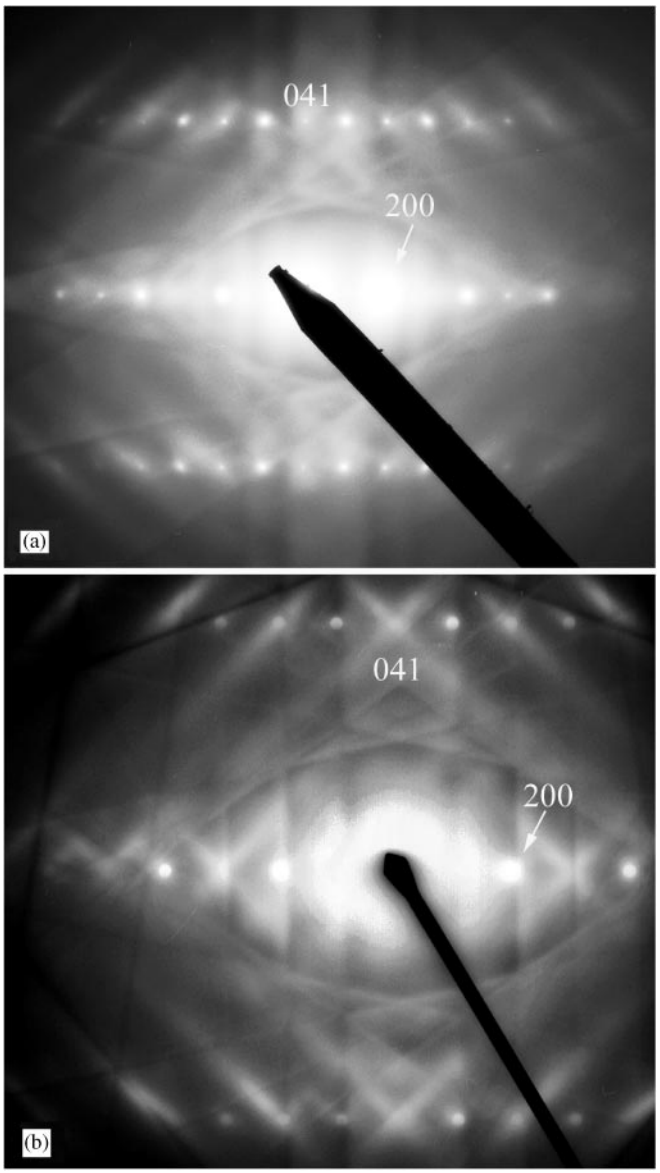

FIG. 3. Typical [0$\bar{1}$4] zone axis EDPs for (a) the solid solution composition $Fe^{II}_{0.24}Fe^{II}_{0.76}O_{0.76}F_{1.24}$ and (b) stoichiometric FeOF. Note the characteristic diffuse is present in both but is less intense and sharp for the solid solution sample.

*SS*2. Figure 3a shows an [0$\bar{1}$4]-type zone axis electron diffraction pattern (EDP), representative of orientations close to [001] for $Fe^{II}_{0.24}Fe^{III}_{0.76}O_{0.76}F_{1.24}$ (i.e., for $x = 0.76$; representative of specimens toward the left-hand end-member composition of the SS2 solid solution, see Fig. 2). Weak polarized lines of diffuse intensity are visible running through the $(h + k + l)$ odd parent reflections approximately along the $\langle 110\rangle$* (i.e., [110]* and [1$\bar{1}$0]*) directions of reciprocal space. Diffuse streaking of this type is characteristic of any composition within the SS2 solid solution region and is in fact essentially the same as the streaking reported previously (7) for stoichiometric FeOF (cf. Fig. 3a with Fig. 3b).

In the latter case, a careful and detailed electron diffraction study showed that the corresponding diffuse distribution took the form of continuous, transverse-polarized rods of diffuse intensity running along both [110]* and [1$\bar{1}$0]* directions of reciprocal space. The crystal chemical origin of these $\langle 110\rangle$*-type diffuse rods was shown to be due to a very specific type of O^{2-}/F^{-} ordering pattern (principally a requirement that opposite vertices of each anion octahedron should not be occupied by anions of the same type—see Fig. 4a) in $\{110\}$-type (i.e., (110) and (1$\bar{1}$0)) planes with no correlation from one such $\{110\}$ plane to the next. This O^{2-}/F^{-} ordering pattern in turn was shown to lead to shifts of the Fe^{3+} ions away from the octahedral centers predominantly along the orthogonal $\langle 1\bar{1}0\rangle$ directions, as shown in Fig. 4a. Given that both $Fe^{III}OF$ and $Fe^{II}_{0.24}Fe^{III}_{0.76}O_{0.76}F_{1.24}$ belong to the same SS2 solid solution, it is only reasonable that correlated O^{2-}/F^{-} ordering and induced Fe^{3+} ion displacements of the same general type as shown in Fig. 4a must be responsible for this first

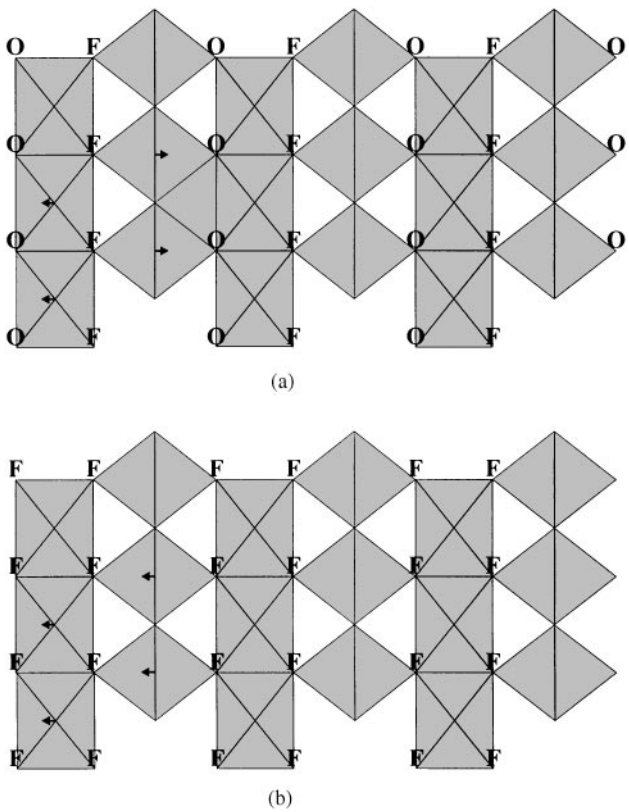

FIG. 4. Schematic representation of the $\{110\}$ planes for the rutile-type structure showing (a) the oxygen/fluorine ordering pattern for FeOF and the induced anticorrelated Fe displacements along $\langle 1\bar{1}0\rangle$ and (b) the shift pattern of Fe as implied by the extinction condition found in the FeF_2 EDPs.

type of observed diffuse distribution and occur right across the whole SS2 solid solution field.

Given, however, that the long-range nature of the O^{2-}/F^- and associated Fe^{3+} displacement pattern within {110} planes (see Fig. 4a) can no longer be maintained as soon as the oxygen/fluorine ratio differs from 1 (i.e., as soon as x decreases from 1), it is not surprising that the diffuse rods for the $Fe^{II}_{0.24}Fe^{III}_{0.76}O_{0.76}F_{1.24}$ composition are rather less intense and certainly rather less sharp than those for $Fe^{3+}OF$ itself (cf. Figs. 3a and 3b).

Upon x being reduced from 1, Fe^{3+} ions begin to be replaced by Fe^{2+} ions while simultaneously the same number of O^{2-} ions are replaced by F^- anions. Any ordering associated with this process should give rise to an additional type of diffuse scattering not present for $Fe^{III}OF$ itself. Tilting the same $Fe^{II}_{0.24}Fe^{III}_{0.76}O_{0.76}F_{1.24}$ SS2 sample to an orientation perpendicular to [001], as shown in the $[3\bar{1}0]$ zone axis EDP of Fig. 5a, revealed additional $[hk0]^*$ diffuse streaking (along [130]* in Fig. 5a) running through the average structure Bragg reflections, which was not present in $Fe^{3+}OF$ itself. Such $[hk0]^*$ diffuse streaking can also be seen in any other orientation for which an $[hk0]^*$ reflection is excited, such as for example the $[3\bar{2}1]$ zone axis EDP shown in Fig. 5b. In this case the diffuse streaking runs along the [230]* direction of reciprocal space. In general, such $[hk0]^*$ diffuse streaking requires the existence of diffuse sheets of intensity perpendicular to c^*.

The implication of this is that there exists medium- to long-range ordering and associated displacive relaxation in one-dimensional columns of atoms along [001] without there being much sideways or lateral correlation in this ordering between neighboring [001] columns. The most plausible explanation for this second type of diffusive distribution is correlated occupancies of the additional Fe^{2+} and F^- ions (associated with reducing x) along one-dimensional columns of edge-connected FeA_6 (A for anion) octahedra running along the [001] direction of the average rutile-type structure (see Figs. 1 and 4a).

Earlier bond valence calculations (Table 1) showed that an Fe^{2+} ion is considerably overbonded in the FeOF average structure (AV = 2.61) when it is surrounded by three O^{2-}'s and three F^-'s. This overbonding can, however, be reduced by $\sim$0.1 valence unit for each O^{2-} replaced by a F^- in the anion octahedra immediately surrounding each additional Fe^{2+} cation. Consideration of Fig. 4a shows that the most efficient way for this to happen would be to cluster the additional Fe^{2+} and F^- ions in strings running along the c direction, so that strings of $[Fe^{II}OF_5]$ octahedra would share edges running along, c, terminating with $[Fe^{II}O_2F_4]$ octahedra at either end before an even longer string of edge-connected $[Fe^{III}O_3F_3]$ octahedra separating them. The observed sheets of diffuse intensity perpendicular to c^* imply that there is little if any lateral correlation in the positioning of these strings from one octahedral column to the next while the clustering along c would be consistent with the diffuse sheets running through the average structure Bragg reflections (see Fig. 5) along c^*.

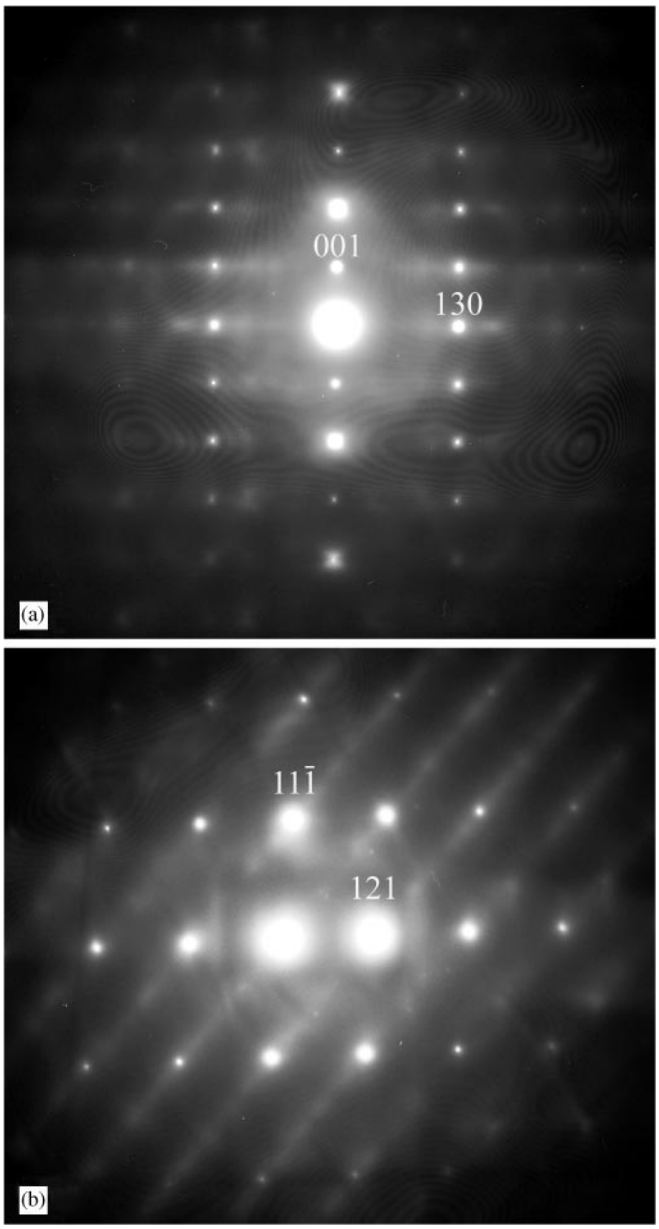

FIG. 5. (a) $[3\bar{1}0]$ and (b) $[3\bar{2}1]$ selected area zone axis orientation EDP of $Fe^{II}_{0.24}Fe^{III}_{0.76}O_{0.76}F_{1.24}$. In each case the diffuse streaking can be seen to occur along $[hk0]^*$ directions of reciprocal space.

Even given the reduction in overbonding implied by strings of edge-connected $[Fe^{II}OF_5]$ octahedra, the Fe^{2+}'s will still be overbonded. Given that they cannot meet their desired valence requirements by shifting from the octahedral center (as for Fe^{3+}), the only option is to expand the octahedron to reduce its local average valence. This is the

local crystal chemical origin of the expanding c axis upon reduction of x. From the point of view of minimizing overall lattice strain, particularly along c, it is then only logical to keep the Fe^{2+}/Fe^{3+} ratio the same within each column along [001]. It is, however, not possible to say more without rather more detailed diffuse scattering data.

*SS*1. Figure 6a shows an EDP close to an [001] zone axis orientation for the SS1 end member composition ($Fe^{II}_{0.92}Fe^{III}_{0.08}O_{0.08}F_{1.92}$). Remarkably, just as for $Fe^{III}OF$, strong lines of transverse-polarized diffuse intensity are again observed to run along the [110]* and [1$\bar{1}$0]* directions of reciprocal space. Note, however, that there has been a fundamental, although subtle, change in the nature of the diffuse distribution. The diffuse streaking is now seen to run only through $(h + k + l)$ even, rather than odd, parent rutile-type reflections (cf. Fig. 6 with Fig. 3). It is clear, nonetheless, that this extinction condition remains body centered in nature and hence requires that Fe^{2+} displacements must make the prime contribution to the observed scattering. The transverse polarized nature of the diffuse streaking in Figs. 6a and 6b, i.e., the fact that the diffuse streaking along either $\langle 110\rangle$* direction is always most intense when looking along the orthogonal $\langle 1\bar{1}0\rangle$* direction of reciprocal space, requires that the responsible displacive shifts must also be perpendicular to the particular $\langle 110\rangle$* rod direction, along the orthogonal $\langle 1\bar{1}0\rangle$* direction of reciprocal space.

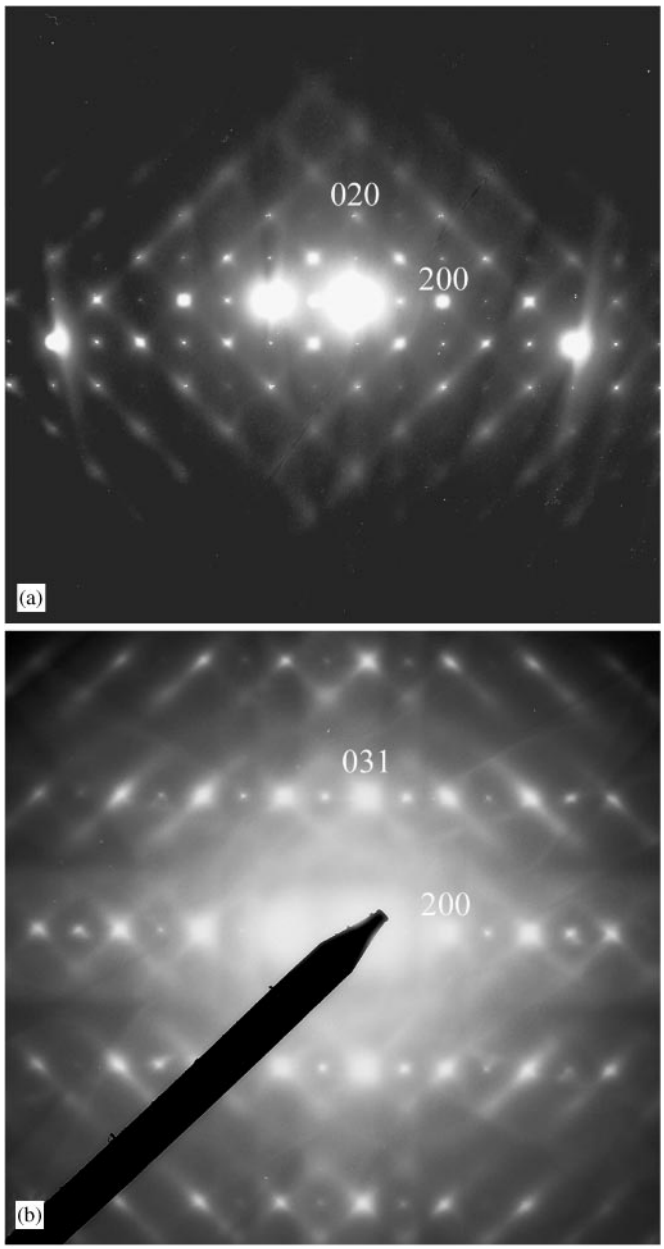

FIG. 6. Selected area EDPs taken (a) close to the [001] zone axis orientation of $Fe^{II}_{0.24}Fe^{III}_{0.08}O_{0.08}F_{1.92}$ and (b) the [0$\bar{1}$3] zone axis orientation for FeF_2. Note the change in extinction condition when compared to the SS2 solid solution samples.

Furthermore, the shifts of the two independent Fe atoms per rutile-type parent unit cell must be correlated, i.e., have the same sign, as a result of the fact that the diffuse streaking this time runs through the $h + k + l =$ even reflections (see (7)). The implied pattern of Fe shifts within each (1$\bar{1}$0) plane is shown in Fig. 4b. The diffuse rod along [1$\bar{1}$0]*, however, requires that there is no correlation in this Fe shift pattern from one such (1$\bar{1}$0) plane to the next.

In the SS2 case, it was possible to attribute the observed Fe shifts to O/F ordering (see Fig. 4a). In the SS1 case, however, it is not possible that oxygen/fluorine ordering could be responsible for these Fe shifts due to the rather limited concentration of oxygen ions involved ($\sim$3%). Furthermore, investigation of the FeF_2 starting material revealed the presence of exactly the same kind of characteristic diffuse intensity distribution. (Indeed it was not possible to detect any difference between EDPs of the SS1 end member composition $Fe^{II}_{0.92}Fe^{III}_{0.08}O_{0.08}F_{1.92}$ and $Fe^{II}F_2$ itself.) Figure 6b, for example, shows an [0$\bar{1}$3] zone axis EDP of FeF_2. The same type of characteristic diffuse intensity distribution is clearly present. Clearly the observed diffuse distribution and implied Fe^{2+} shift pattern are characteristic of $Fe^{II}F_2$ itself.

The refined anisotropic thermal parameters of $Fe^{II}F_2$ are reasonably isotropic (8, 14) and do not provide any supporting evidence for the correlated anisotropic Fe^{2+} shift pattern shown in Fig. 4b. They do, however, limit the possible magnitude of these Fe^{2+} shifts to $< \sim 0.1$ Å. Exactly why these particular transverse-polarized phonon modes (see Fig. 4b) should be close to being soft is an intriguing question but beyond the scope of the current contribution.

REFERENCES

1. J. Ravez, *J. Phys. III Fr.* **7,** 1129–1144 (1997).
2. P. Hagenmuller, *in* "Perspectives in solid state chemistry" (K. J. Rao, Ed.), pp. 66–78. Narosa, New Delhi, 1995.
3. L.-S. Du, F. Wang, and C. P. Grey, *J. Solid State Chem.* **140,** 285–294 (1998).
4. T. Vogt, P. M. Woodward, B. A. Hunter, A. K. Prodjosantoso, and B. J. Kennedy, *J. Solid State Chem.* **114,** 228–231 (1999).
5. B. L. Chamberland and A. W. Sleight, *Solid State Commun.* **5,** 765–767 (1967).
6. B. L. Chamberland, A. W. Sleight, and W. H. Cloud, *J. Solid State Chem.* **2,** 49–54 (1970).
7. F. J. Brink, R. L. Withers, and J. G. Thompson, *J. Solid State Chem.* **155,** 359–365 (2000).
8. W. Jauch, A. Palmer, and A. J. Schultz, *Acta Crystallogr. B* **49,** 984–987 (1993).
9. P. Hagenmuller, J. Portier, J. Cadiou, and R. dePape, *C. R. Acad. Sci.* **260,** 4768 (1965).
10. N. N. Greenwood and A. Earnshaw, "Chemistry of the Elements," p. 820. Reed Educational and Professional Publishing Ltd., Oxford, 1997.
11. M. Love and V. D. Scott, *Scanning* **4,** 11–130 (1981).
12. A. R. West, "Solid State Chemistry and its applications," p. 366. Wiley, New York, 1984.
13. N. E. Brese and M. O'Keeffe, *Acta Crystallogr. B* **47,** 192 (1991).
14. M. J. M. de Almeida, M. M. R. Costa, and J. A. Paixão, *Acta Crystallogr. B* **45,** 549–555 (1989).
15. M. Vlasse, J. Massies, and G. Demazeau, *J. Solid State Chem.* **8,** 109 (1973).
16. R. L. Withers, S. Schmid, and J. G. Thompson, *Prog. Solid State Chem.* **26,** 1 (1998).